

ARTICLE OPEN



Reconfiguration of functional brain hierarchy in schizophrenia

Irene Acero-Pousa ^{1,2,✉}, Anira Escrichs ¹, Paulina Clara Dagnino ^{1,2}, Yonatan Sanz Perl ^{1,2,3}, Morten L. Kringelbach ^{2,4,5,6}, Peter J. Uhlhass ^{7,8} and Gustavo Deco ^{1,2,9}

© The Author(s) 2025

The multidimensional nature of schizophrenia requires a comprehensive exploration of the functional and structural brain networks. While prior research has provided valuable insights into these aspects, our study goes a step further to investigate the reconfiguration of the hierarchy of brain dynamics, which can help understand how brain regions interact and coordinate in schizophrenia. We applied an innovative thermodynamic framework, which allows for a quantification of the degree of functional hierarchical organisation by analysing resting state fMRI-data. Our findings reveal increased hierarchical organisation at the whole-brain level and within specific resting-state networks in individuals with schizophrenia, which correlated with negative symptoms, positive formal thought disorder and apathy. Moreover, using a machine learning approach, we showed that hierarchy measures allow a robust diagnostic separation between healthy controls and schizophrenia patients. Thus, our findings provide new insights into the nature of functional connectivity anomalies in schizophrenia, suggesting that they could be caused by the breakdown of the functional orchestration of brain dynamics.

Translational Psychiatry (2025)15:356; <https://doi.org/10.1038/s41398-025-03584-0>

INTRODUCTION

Schizophrenia is a severe and often chronic psychiatric disorder characterized by a range of multidimensional symptoms, including positive symptoms, such as hallucinations and delusions, and negative symptoms, such as anhedonia and avolition [1]. The multifaceted nature of schizophrenia is further compounded by fluctuating symptomatology throughout individuals' lives, leading to significant heterogeneity among patients [2]. This complexity and variability require a comprehensive exploration of both the anatomical and functional brain networks.

The presence of neuroanatomical anomalies in both grey and white matter is a well-established phenomenon in schizophrenia [3, 4]. Robust evidence has revealed regionally decreased grey matter in both first-episode and chronic schizophrenia patients, specifically in the frontal lobe [5–7], cingulate cortex [5, 8], the thalamus [9, 10], insula [11], post-central gyrus [5], and medial temporal regions [5, 6]. In terms of white matter alterations, reductions in the corpus callosum [8], as well as in the frontal and temporal lobes [8, 12] have been extensively documented.

Furthermore, alterations in functional brain dynamics in schizophrenia have been thoroughly reported using resting-state functional magnetic resonance imaging (fMRI) [13, 14]. Among the networks considered most relevant are the salience network and the default mode network (DMN) [15, 16]. Studies have identified heterogeneous findings, with some indicating hyperconnectivity [17, 18], while others report hypoconnectivity [19] which can vary across networks [20–22].

Despite the numerous identified structural and functional abnormalities, the underlying nature of the pathophysiology remains unclear [23], emphasizing the need for alternative perspectives and hypotheses. One promising approach to conceptualize these anomalies is to consider these deficits as a disorder of integration of information across brain regions [24–27]. Information integration can be studied by analysing the level of asymmetry in the interactions among brain regions, that is, the extent to which information is transmitted in a non-reciprocal manner between them. In a symmetrical system, communication between regions is reciprocal, with no dominant directionality, leading to a uniform distribution of information processing. However, this lacks the differentiation needed for hierarchical organisation, where certain regions play specialized or more influential roles in guiding brain function. On the other hand, asymmetrical interactions indicate non-reciprocal communication, where information is integrated in a small group of regions before being transmitted to the others across the whole-brain [28, 29]. This creates a hierarchical arrangement that is indicative of non-equilibrium systems, facilitates distinct processing of specialized functional domains and allows for dynamic configuration and intercommunication among brain regions [30, 31].

Hierarchical organisation in fMRI-data has been previously assessed in several studies. For instance, previous studies have revealed that states of reduced consciousness exhibit lower hierarchical arrangements compared to conscious wakefulness [32, 33]. Moreover, physically and cognitively demanding tasks

¹Computational Neuroscience Group, Center for Brain and Cognition, Department of Information and Communication Technologies, Universitat Pompeu Fabra, Barcelona, Spain. ²International Centre for Flourishing, Universities of Oxford (UK), Aarhus (Denmark) and Pompeu Fabra (Spain), Oxford, UK. ³Department of Engineering, University of San Andrés, Buenos Aires, Argentina. ⁴Department of Psychiatry, University of Oxford, Oxford, UK. ⁵Center for Music in the Brain, Department of Clinical Medicine, Aarhus University, Aarhus, Denmark. ⁶Centre for Eudaimonia and Human Flourishing, Linacre College, University of Oxford, Oxford, UK. ⁷Department of Child and Adolescent Psychiatry, Charité-Universitätsmedizin Berlin, Berlin, Germany. ⁸Institute of Neuroscience and Psychology, University of Glasgow, Glasgow, Scotland, United Kingdom of Great Britain and Northern Ireland. ⁹Institució Catalana de la Recerca i Estudis Avançats (ICREA), Barcelona, Spain. ✉email: irene.aceroi@upf.edu

Received: 13 May 2025 Revised: 29 July 2025 Accepted: 28 August 2025

Published online: 06 October 2025

increase the hierarchical organisation compared to a resting state [34, 35]. In the context of schizophrenia, some studies suggest overall altered hierarchy [36–40], while others highlight specific alterations in individual networks [41–43].

Here, we apply a new theoretical framework able to quantify the hierarchical organisation of brain networks in schizophrenia [44]. The core idea is that the level of hierarchy in a system is reflected in how far it deviates from thermodynamic equilibrium [28]. To capture this, we use the fluctuation-dissipation theorem (FDT) from statistical physics, in combination with whole-brain modeling [45, 46]. At equilibrium, a system's spontaneous fluctuations can accurately predict its response to small perturbations, a principle formalized by FDT. In contrast, non-equilibrium systems violate this principle: their intrinsic fluctuations fail to predict dissipation after perturbations. The magnitude of these violations serves as a proxy for the level of non-equilibrium, which in turn reflects the system's hierarchical organisation [44]. This is because hierarchical systems are inherently directional: information flows preferentially from higher to lower levels, introducing asymmetries that push the system away from equilibrium.

We apply this framework to investigate whether individuals with schizophrenia exhibit altered hierarchical dynamics. We hypothesize that in schizophrenia, the flow of information across brain regions is disrupted, leading to a breakdown in the orchestrated coordination that underlies healthy brain function. Furthermore, we hypothesize that the degree of hierarchical organisation correlates with symptom severity across individuals.

MATERIALS AND METHODS

Participants

In this study, we analysed resting-state fMRI data sourced from the UCLA Consortium for Neuropsychiatric Phenomics LA5c Study [47], openneuro.org/datasets/ds000030. Our participant pool encompassed two age-matched cohorts: 50 individuals diagnosed with schizophrenia (12 female, mean group age: 36.5 ± 8.8 , standard error of the mean (SEM) ± 1.26) and 50 healthy subjects (16 female, mean group age: 36.6 ± 8.9 , SEM ± 0.88). All participants provided written informed consent following the University of California Los Angeles Institutional Review Board's approved protocols. Control group inclusion criteria involved individuals with no prior psychiatric diagnoses or familial psychiatric history and no prior exposure to psychotropic drugs. Detailed dataset information is available in the data description provided by Poldrack et al. [48].

Functional MRI data acquisition

MRI data was acquired using two distinct scanners, the Ahmanson-Lovelace Brain Mapping Center (Siemens version syngo MR B15) and the Staglin Center for Cognitive Neuroscience (Siemens version syngo MR B17) at UCLA. Functional MRI data was collected using a T2* weighted echoplanar imaging sequence with oblique slice orientation (slice thickness = 4 mm, 34 slices, TR = 2 s, TE = 30 ms, flip angle = 90° , matrix 64×64 , FOV = 192 mm, 152 volumes). An anatomical volume was also captured using a T1-weighted sequence (TR = 1.9 s, TE = 2.26 ms, FOV = 250 mm, matrix = 256×256 , sagittal plane, slice thickness = 1 mm, 176 volumes). Throughout the experiment, participants were instructed to remain relaxed with their eyes open.

Preprocessing of the fMRI data involved fMRIPrep v1.1 [49], a Nipype-based tool developed by Gorgolewski et al. [50]. Motion-related noise was removed using the nonaggressive variant of ICA-AROMA [51], which preserves shared variance between motion- and neural-related components while regressing out only motion-specific variance. Additionally, mean white matter and cerebrospinal fluid signal were regressed out and no global signal regression (GSR) was utilized during data processing. Finally, the brain was divided using the DK80 parcellation [52], including 62 cortical (31 per hemisphere), and 18 subcortical areas (9 per hemisphere), a total of 80 regions.

Diffusion MRI data acquisition

For structural connectivity data acquisition, we processed multi-shell diffusion-weighted imaging (DWI) data from a separate normative sample of 32 healthy participants drawn from the Human Connectome Project

(HCP) database. These data were used solely to generate the structural connectivity matrix for the whole-brain model and were not derived from the same individuals included in the main experimental analyses. The scans, spanning approximately 89 min, adhered to acquisition parameters detailed in Thomas et al. [53]. Connectivity was estimated using the method outlined by Horn et al. [54]. Briefly, the data was processed using a generalized q-sampling imaging algorithm implemented in DSI studio (<http://dsi-studio.labsolver.org>). T2-weighted anatomical images were segmented to generate a white-matter mask, and image co-registration to the b0 image of the diffusion data was performed employing SPM12. Within this refined white-matter mask, we sampled 200,000 fibres for each participant in the Human Connectome Project. These fibres were then transformed into MNI space, utilizing Lead-DBS [55]. The methodology was designed to employ algorithms demonstrated to be optimal, minimizing false-positive fibres, as underscored in recent open challenges [56, 57].

Theoretical framework

Violations of the fluctuation-dissipation theorem. To characterize the degree of non-equilibrium in brain dynamics, we quantify violations of the Fluctuation-Dissipation Theorem (FDT) [44]. In essence, the FDT formalizes a core principle of thermodynamic equilibrium: in systems that are in equilibrium, the internal fluctuations (random, spontaneous changes) contain all the information needed to predict how the system would respond to small perturbations. This relationship breaks down in systems that are out of equilibrium, such as living organisms or brain networks, because these systems are not random and spontaneous anymore but exhibit directional, asymmetric, and history-dependent behaviors. As a result, the actual response to perturbation deviates from what would be predicted based on fluctuations alone, leading to a violation of the FDT. Thus, the level of violation of the FDT is indicative of the degree of non-equilibrium in a system, which we use as a proxy of the level of hierarchy [44]. The underlying rationale is that hierarchically organized systems exhibit asymmetric and directional information flow, which is a hallmark of non-equilibrium.

To quantify these violations, we rely on Onsager's regression principle, which offers a conceptual and mathematical foundation for the FDT [45, 58]. Onsager postulated that the relaxation of a system back to equilibrium after a small perturbation follows the same trajectory as a spontaneous fluctuation would in an unperturbed system. This symmetry between cause and effect enables the derivation of FDT and provides a way to measure its violations.

Let us consider a system initially in equilibrium (state 1), with its fluctuations described by a probability distribution $P_0(G)$, where G represents a configuration of the system (e.g., a brain state). At time $t = 0$, we apply a small perturbation ϵ coupled to an observable $B(G)$, causing the system to transition toward a new configuration (state 2). We then monitor the evolution of another observable $A(G)$ over time. The expected value of A at time t is given by:

$$\langle A(t) \rangle_\epsilon = \sum_{G, G_0} A(G) P_\epsilon(G, t | G_0, 0) P_0(G_0). \quad (1)$$

Here, $P_\epsilon(G, t | G_0, 0)$ is the conditional probability that the system evolves from configuration G_0 to G over time t . In this expression, we average over all possible initial configurations G_0 , each weighted by their likelihood at equilibrium $P_0(G_0)$ to compute the expected value of observable A after time t , depending on how the system evolves from each G_0 .

Intuitively, this can be seen as applying a perturbation to a brain area B and observing its effects on another brain area A . According to Onsager's regression hypothesis, the system's response to a weak perturbation mirrors the way it would spontaneously fluctuate when unperturbed. In other words, the relaxation of the system after a disturbance follows the same statistical patterns as its natural fluctuations at equilibrium. Using this principle, we can rewrite the conditional probability $P_\epsilon(G, t | G_0, 0)$ in terms of the system's equilibrium dynamics, and a correction due to the perturbation:

$$P_\epsilon(G, t | G_0, 0) = P_0(G, t | G_0, 0) \exp(\beta \epsilon [B(G) - B(G_0)]). \quad (2)$$

Here, $P_0(G, t | G_0, 0)$ is the unperturbed conditional probability, that is, how the system would evolve from configuration G_0 to G over time t when it is not perturbed, ϵ is the strength of the perturbation, $B(G)$ is the observable it acts on, and $\beta = \frac{1}{k_B T}$ is the inverse of the temperature, from statistical mechanics, which reflects how sensitive the system is to changes at a given temperature. Essentially, this equation says that the perturbed

conditional probability equals the unperturbed probability slightly modified by how strongly the perturbation influences the system. Substituting this into Eq. 1 and expanding the exponential to first order in ε , we obtain:

$$\begin{aligned} \langle A(t) \rangle_\varepsilon - \langle A(t) \rangle_0 &= \beta \varepsilon \sum_{G, G_0} A(G)[B(G) - B(G_0)]P_0(G_0) \\ &= \beta \varepsilon [\langle A(t)B(t) \rangle_0 - \langle A(t)B(0) \rangle_0] \end{aligned} \quad (3)$$

Which indicates that the change in the expectation value of A due to a small perturbation in B is governed by how A and B are spontaneously correlated in the unperturbed system.

Then, we can define the susceptibility as the change in the expectation value of A in response to the perturbation. This measures how sensitive A is to changes in B , and is formally given by the derivative of $\langle A(t) \rangle$ with respect to the perturbation strength ε :

$$\chi_{A,B}(t) = \frac{\partial \langle A(t) \rangle}{\partial \varepsilon} = \frac{\langle A(t) \rangle_\varepsilon - \langle A(t) \rangle_0}{\varepsilon} = \beta [\langle A(t)B(t) \rangle_0 - \langle A(t) \rangle_0 \langle B(t) \rangle_0] \quad (4)$$

This expression indicates that the susceptibility at time t depends entirely on correlation functions of the unperturbed system.

To obtain the static form of the FDT, we consider the limit where the system has had enough time to relax after the perturbation, that is when $t \rightarrow \infty$, obtaining the correspondence between the response of a system to a perturbation (on the left-hand side) and its unperturbed correlations (on the right-hand side) in equilibrium:

$$\chi_{A,B} = \beta [\langle AB \rangle_0 - \langle A \rangle_0 \langle B \rangle_0] \quad (5)$$

Violations of the FDT in non-equilibrium. If we describe the unperturbed state to have the mean values of the observables equal to zero ($\langle A \rangle_0 \langle B \rangle_0 = 0$), then we can characterize the level of non-equilibrium as the normalized divergence of a system from the FDT:

$$D_{A,B} = \frac{\beta \langle AB \rangle_0 - \chi_{A,B}}{\chi_{A,B}}, \quad (6)$$

where $\beta \langle AB \rangle_0$ explains the unperturbed fluctuations and $\chi_{A,B}$ corresponds to the response to a small perturbation ε . To obtain the total deviation of the FDT (D), we need to compute the mean value of $D_{A,B}$ for all observables A and all perturbation points B . Thus, by leveraging the degree of deviation from the FDT we are assessing the distance from equilibrium of a system.

Model-based FDT of whole-brain data

Whole-brain model. In order to estimate the total violation of the FDT (D , Eq. 6), we need to systematically perturb all brain regions B and observe the respective responses on all brain regions A . Thus, our initial step involves constructing a whole-brain model fitting the functional neuroimaging data in each group. This model allows us to derive the analytical expressions elucidating the correlations among all brain regions under spontaneous fluctuations and, subsequently, to apply a perturbation in a brain region and predict their average effect in all the other regions.

The whole-brain model consists of describing each node's local dynamics as the normal form of a supercritical Hopf bifurcation, capable of defining the transition from asynchronous noisy behaviour to oscillations [59]. Please, see the Supplementary Information (SI) for the full mathematical description of the Hopf model and its linearization. Details on the model parameters are provided in Supplementary Table 4.

Measuring violations of the model-based FDT. Using the described model, we can compute the violations of the FDT. First, we start by computing the covariance matrix $K = \langle \delta u \delta u^T \rangle$. To do it, we first express Eq. 3 (SI) as $d\delta u = J\delta u dt + dW$, where dW stands for a Wiener process with covariance $\langle dW dW^T \rangle = Q dt$. Here, Q is the covariance matrix of the noise. Then, using Itô's stochastic calculus, we obtain $d(\delta u \delta u^T) = d(\delta u) \delta u^T + \delta u d(\delta u^T) + d(\delta u) d(\delta u^T)$. Considering that $\langle \delta u dW^T \rangle = 0$, maintaining the terms to first order in the differential dt and taking the expectations, we get:

$$\frac{dK}{dt} = JK + KJ^T + Q. \quad (7)$$

This allows us to compute the static covariance by

$$JK + KJ^T + Q = 0, \quad (8)$$

which can be solved using the eigen-decomposition of the Jacobian matrix J [60] and, from the first N rows and columns of the covariance K we finally get the functional connectivity simulated by the model ($FC^{simulated}$), which represents the real part of the dynamics.

Having a fitted coupling matrix C for each participant and each group (see SI), we formulate an analytical expression of Eq. 6 for the deviation from the FDT. Initially, we compute the expectation values of the state variables $\langle \delta u \rangle_{ej}$ when a perturbation ε is applied to a node j . Utilizing Eq. 3 (SI), we can determine that $\frac{d}{dt} \langle \delta u \rangle_{ej} = J \langle \delta u \rangle_{ej} + h_j = 0$, being h_j a $2N$ vector primarily of zeros except component j that equals the value of the perturbation ε . Solving for the desired expectation value, we obtain $\langle \delta u \rangle_{ej} = -J^{-1} h_j$. Considering only the real part of $\langle \delta u \rangle_{ej}$, we obtain $\langle \delta x \rangle_j = \langle \delta x \rangle_{ej}^{\text{re}}$. With this, we proceed to define the deviation from the FDT for region i when a perturbation is applied to region j :

$$D_{i,j} = \frac{2 \langle \delta x_i \delta x_j \rangle_{\frac{\partial}{\partial \varepsilon}} - \langle \delta x_i \rangle_j}{\langle \delta x_i \rangle_j} \quad (9)$$

Here, the covariance $\langle \delta x_i \delta x_j \rangle_0$ is computed from $K^{simulated}$, and the term $\frac{\partial}{\partial \varepsilon}$ is the inverse of temperature β . Then, the effect of perturbing region j on all the other regions can be computed as:

$$P_j = \frac{\frac{1}{N} \sum_i 2 \langle \delta x_i \delta x_j \rangle_{\frac{\partial}{\partial \varepsilon}} - \langle \delta x_i \rangle_j}{\frac{1}{N} \sum_i \langle \delta x_i \rangle_j} \quad (10)$$

With this equation, we can define a vector, the perturbability map P which quantifies the global impact of each region's perturbation. This perturbability reflects how strongly a region drives the system's dynamics out of equilibrium, serving as a proxy for hierarchical position. Regions exhibiting stronger violations of the fluctuation-dissipation theorem (FDT) are considered higher in the functional hierarchy, exerting intrinsic and directional influence beyond symmetric equilibrium dynamics. Conversely, regions with minimal FDT violations rank lower, with dynamics primarily shaped by incoming interactions.

This hierarchical interpretation is grounded in the fact that FDT violations emerge from asymmetric, directional interactions between regions. Specifically, regions with higher FDT deviation show a characteristic asymmetry: a greater out-degree (number of outgoing connections) combined with a lower in-degree (number of incoming connections). This imbalance reflects their net directional influence, enabling these regions to drive the system farther from equilibrium. Therefore, larger departures from equilibrium correspond to stronger asymmetry, which underpins the preferential flow of information that defines functional hierarchy (Supplementary Fig. 1).

Using it, we can compute the level of non-equilibrium for each participant by averaging the deviation from the FDT over all possible perturbations:

$$D^\wedge = \frac{1}{N} \sum_j P_j \quad (11)$$

The analysis across the whole-brain network is performed both at the subject and at the node level. In the first case, we compute D^\wedge for each participant belonging to each group, obtaining one average value of FDT deviations of cortical nodes per subject. In the second case, we average the perturbability maps P across subjects in each group, obtaining one averaged P per group, which represents the mean value per node.

Resting-state networks

Resting-state networks (RSNs) were defined using a canonical atlas-based approach, previously reported in [61]. Each brain region from our parcellation was spatially mapped onto the canonical Yeo 7-network atlas in MNI space [62]. For each region, we calculated the fractional overlap with each of the seven RSNs. The region was then assigned exclusively to the RSN with which it had the highest fractional overlap.

Support vector machine classification

We trained an SVM classifier to distinguish between subjects in each group, using as input the perturbability maps. Subsequently, we assessed classifier performance using four distinct SVM linear models. These classifiers were trained on different input data, specifically: functional connectivity (FC) derived from empirical data, effective connectivity (EC) computed within the optimised whole-brain model, FDT deviations, and a combination of EC and FDT deviations. The distinct inputs were z-scored

before being passed into the model. To ensure consistent input dimensionality, we repeated the assessment of classifier performance using the four inputs, performing a Principal Component Analysis on each and using the 10 first principal components for the model. To further assess the contribution of temporal dynamics, we implemented a sliding-window approach (window size = 50 time points, overlap = 25) to compute dynamic versions of FC, EC, and FDT. For each window, FC was calculated directly, and whole-brain models were fitted to estimate EC and FDT deviations over time. PCA was again applied to the resulting dynamic features, and the first ten components were used for classification. In all cases, the training process involved utilizing 80% of the dataset, while the accuracy was evaluated on the remaining 20% across 1000 k-folds. The SVM used a linear kernel with automatic scaling and a box constraint of 2.5. Furthermore, a detailed analysis was conducted on the model exhibiting the highest accuracy to comprehend its feature importance. This involved extracting the coefficients of the model, sorting them from highest to lowest, and selecting the top 5. These top coefficients correspond to specific nodes within the brain parcellation, elucidating the significant brain regions driving the classification.

Exploratory factor analysis

We follow the methodology in Schöttner et al. [63] to reduce the dimensionality of our behavioral dataset. Using the “Factor Analyzer” package implemented in Python (https://github.com/EducationalTestingService/factor_analyzer), we focus our analysis on variables from the Scale Analysis of Positive Symptoms (SAPS) and Scale Analysis of Negative Symptoms (SANS) that have less than 10% missing values. Prior to the analysis, all variables are standardized (z-scored) across subjects. The “Factor Analyzer” package facilitates dimensionality reduction by extracting underlying factors from the dataset. This process results in the identification of three factors, each comprising loadings for individual variables and scores for each subject. These factors represent distinct dimensions of symptomatology within our dataset.

Statistical analysis

To gain insight into the differences in FDT deviation between individuals with schizophrenia and the control cohort, we employ the non-parametric independent-sample Mann-Whitney U test with 10000 permutations. To understand the relationship between FDT deviation and symptom severity, we conduct correlation analysis between the standard deviation of the FDT deviation values across brain regions per subject and the scores obtained in each factor. In all analyses, significance is established for p-values below 0.05. For the analysis conducted between groups at the RSNs level and for the correlations with the symptomatology, we implement the False Discovery Rate (FDR) correction method to account for multiple comparisons [64]. The p-values outlined are the ones obtained after FDR correction. Preceding all the statistical analyses, outliers are excluded from the comparison, with outliers defined as data points deviating more than three standard deviations from the mean.

RESULTS

Our study applies a new model-based thermodynamic framework that builds upon the FDT, offering a unique perspective on non-equilibrium brain dynamics and, ultimately, to the hierarchical organisation of the brain [44] (Fig. 1a). The FDT establishes a relationship between the response of a perturbed system to an external force and the internal fluctuations of the same system in the absence of the disturbance [46]. In a non-equilibrium system, these intrinsic fluctuations are inaccurate in predicting the dissipation post-perturbation, leading to a violation of the FDT [45] (Fig. 1b). Hence, an elevated deviation from the FDT signifies a greater degree of non-equilibrium, reflecting more asymmetric interactions between states and, consequently, a heightened level of hierarchical organisation [35, 44, 65, 66]. Building on this principle, our model-based FDT framework combines empirical data and whole-brain modelling to quantify perturbation responses (Fig. 1c).

Hierarchical reconfiguration across the whole-brain

We initially assessed the difference in hierarchical organisation between schizophrenia and control groups at the whole-brain level by leveraging the level of FDT deviations in each participant.

At the whole-brain level, FDT deviation was significantly increased in schizophrenia patients compared to the healthy control group ($p < 0.01$, median (interquartile range (IQR)) = schizophrenia = 39.75 (32.85), controls = 26.62 (23.74)), suggesting an overall increase in hierarchical brain organisation in the disease (Fig. 2a).

Additionally, we explored the hierarchical organisation for each brain area instead of each subject, aiming to provide insights into the specific regions implicated in the observed differences and mitigate the potential confounding effects of individual variability. We computed the degree of FDT deviation for each brain area (i.e., for each group, the average of the perturbability map value across all subjects for each brain region) (see Fig. 2b). Statistical comparisons demonstrated a significantly increased level of FDT deviations in schizophrenia ($p < 0.001$, median (IQR): schizophrenia = 45.47 (14.78), controls = 34.72 (11.71)) (Fig. 2b). Subsequently, we examined the consistency of FDT deviation values among brain areas within each group to determine whether the elevated FDT deviation was associated with specific regions or reflected a more generalized pattern. For this analysis, we calculated the standard deviation (SD) of FDT deviation values across all regions for each group, revealing higher statistically significant values in schizophrenia ($p < 0.001$, median (IQR): schizophrenia = 35.54 (12.58), controls = 26.45 (15.09)) (Fig. 2c). This observation indicates that controls exhibit greater uniformity in the deviation of FDT across brain areas, suggesting that the increased whole-brain FDT values observed in schizophrenia may stem from specific regions with notably higher FDT levels. This localized elevation contributes to the increased variance observed within the schizophrenia group.

To further examine whether FDT deviation distinguishes between schizophrenia subjects and controls, we developed a support vector machine (SVM) classification model. The model was trained using the perturbability map of each subject as input features and achieved an accuracy of 82.5% (Fig. 2d), indicating that the hierarchical organisation can serve as a promising model-based biomarker.

Hierarchical reconfiguration across resting-state networks

To investigate the localization of the alterations, we investigated the FDT deviations across eight resting-state networks (RSNs): the visual, somatomotor, dorsal attention, salience, limbic, control, DMN and subcortical networks. As in the whole-brain assessment, we conducted the analysis both at the subject/single-participant perspective and the brain region perspective.

At the single-participant level, findings reveal a persistent increased FDT deviation in schizophrenia across all RSNs (Fig. 3a). Statistically significant differences emerge in the, somatomotor ($p < 0.01$), dorsal attention ($p < 0.01$), limbic ($p < 0.001$), control ($p < 0.01$), DMN ($p < 0.05$) and subcortical ($p < 0.01$) networks. However, no significance is found in the salience ($p > 0.05$) and visual ($p > 0.05$) networks. All reported p-values were corrected for multiple comparisons using FDR correction (see Supplementary Table 1).

At the brain area level, results also indicate a consistent pattern of elevated FDT deviation within schizophrenia across all RSNs (Fig. 3b). Notably, statistically significant differences appear in the somatomotor ($p < 0.01$), dorsal attention ($p < 0.05$), salience ($p < 0.05$), limbic ($p < 0.01$), control ($p < 0.01$), DMN ($p < 0.05$) and subcortical ($p < 0.01$) networks. Results do not indicate significance in the visual network ($p > 0.05$). All significant p-values persist following FDR correction for multiple comparisons (see Supplementary Table 2).

We represented the mean FDT deviation values of all subjects for each RSN and each group on a uniform scale, aiming to identify the regions with the largest differences in hierarchical organisation between the two groups (Fig. 3c). The findings indicate that the regions orchestrating the changes in hierarchical configuration are the somatomotor (standardized mean difference

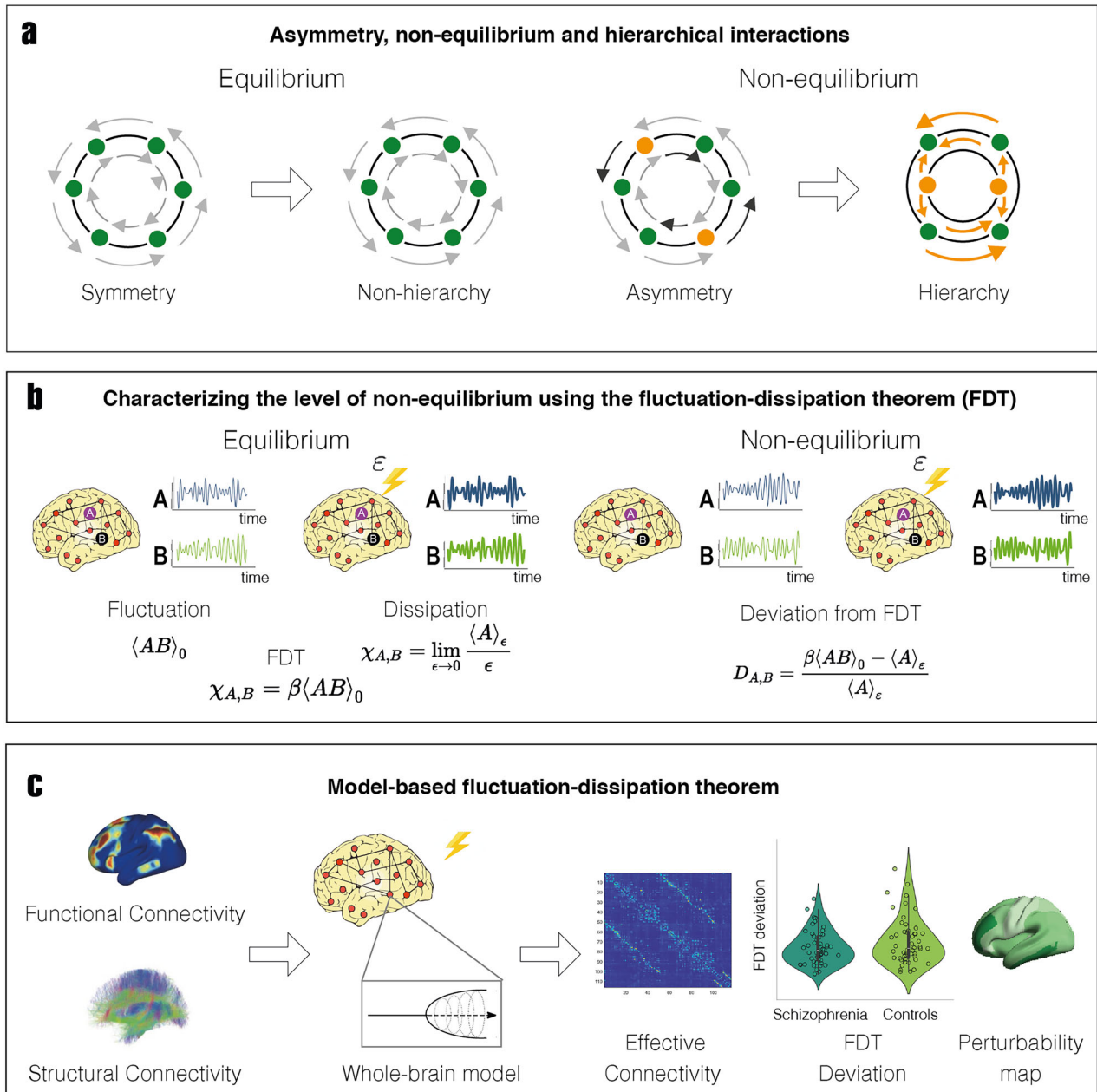


Fig. 1 Capturing the hierarchical organisation using the FDT. **a** Hierarchical level is determined by the level of asymmetry of causal interactions between brain regions arising from the breaking of the detailed balance in a system. In equilibrium, the interaction of brain regions is symmetrical, that is, information flows in a reciprocal manner. These symmetrical relationships are in detailed balance, leading to a non-hierarchical organisation. In contrast, in non-equilibrium, the asymmetrical interactions break the detailed balance, introducing hierarchical organisation in the system. **b** The level of non-equilibrium can be measured by the deviation of FDT, which can then be employed to characterize the hierarchical organisation. In an equilibrium system, spontaneous fluctuations predict the dissipation following the perturbation. Nevertheless, in a non-equilibrium system, the intrinsic fluctuations are not able to forecast the dissipation after a perturbation, leading to a violation of the FDT. **c** FDT is combined with a whole-brain model fitted to empirical neuroimaging data, incorporating functional and structural connectivity. Each node's local dynamics of the model is described as the normal form of a supercritical Hopf bifurcation. The optimised model provides the effective connectivity, the FDT deviations as well as the perturbability maps for different brain states.

(SMD) = 0.67), the subcortical (SMD = 0.60) and the limbic (SMD = 0.57) networks, followed by the control (SMD = 0.51), the salience (SMD = 0.45), the DMN (SMD = 0.44), the dorsal attention (SMD = 0.27) and finally the visual (SMD = 0.21) network (see Supplementary Table 3).

Hierarchical reconfiguration correlates with symptom severity
Next, we explored the potential correlation between the changes of the hierarchical organisation in schizophrenia and

specific symptoms. We employed exploratory factor analysis to reduce the dimensionality of the symptom's data from 58 to 3 factors. The analysis revealed a positive significant correlation between the standard deviation of each subject brain region's FDT deviations and Factor 1 (related to negative symptoms) ($r = 0.32$, $p < 0.05$), a negative significant correlation with Factor 3 (associated with features of positive formal thought disorder and apathy) ($r = -0.31$, $p < 0.05$), but no significant correlation with Factor 2 (characterized by positive symptoms) ($r = -0.27$,

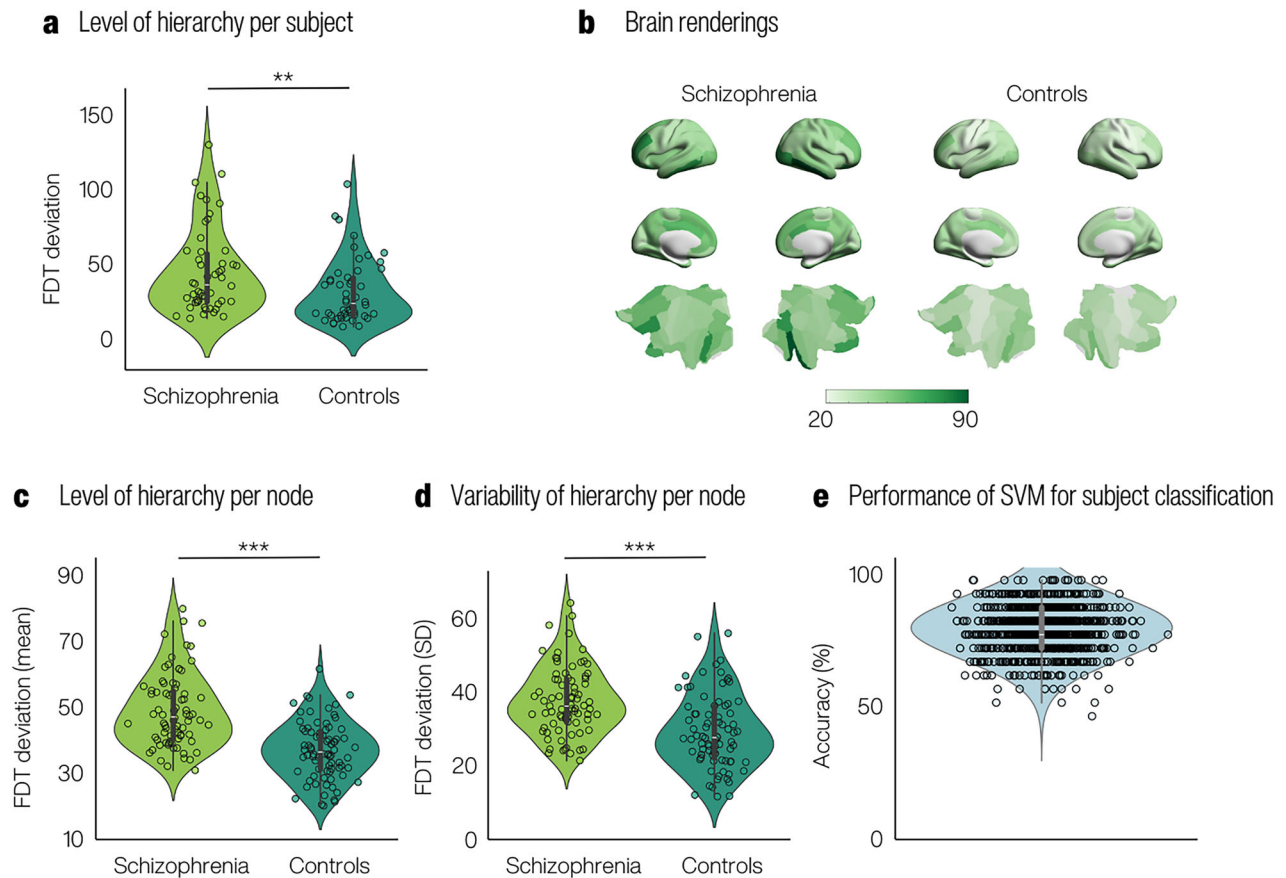


Fig. 2 In schizophrenia, the hierarchical organisation increases as shown by the increase in FDT deviation values across the whole-brain. Analysis of the whole-brain FDT deviation values between schizophrenia and control patients, to understand differences in hierarchical brain organisation. **a** Boxplots illustrate the distribution of the average FDT values per subject **b** Boxplots show the distribution of the average FDT values per node, obtained by averaging each brain area in the perturbability map across subjects. **c** Boxplots depict the distribution of the standard deviation of the perturbability map across nodes. **d** The violin plot displays the distribution of the support vector machine model's accuracy across 1000 k-folds using the perturbability map of each subject as input. **e** Brain renders represent the spatial distribution of the average FDT values per node for each group. Asterisks in the figure indicate statistical significance: ** represents $p < 0.01$ and *** represents $p < 0.001$.

$p > 0.05$) (Fig. 4). The reported p -values are the ones obtained after correcting for multiple comparisons using FDR. Additionally, we examined the correlation between the average FDT deviation and each of the three symptom factors. These analyses did not reveal any significant associations (all p -values > 0.05).

To further explore these relationships, we performed an analysis of hierarchical organisation in brain areas associated with each symptom factor. For each factor identified through dimensionality reduction, we compared the perturbability maps of subjects with high and low factor scores to identify brain areas with the largest differences in hierarchical organisation. Subjects were split based on the median: those with scores below the median were classified as having low factor scores, while those with scores above the median were classified as having high factor scores. For Factor 1 (negative symptoms), the most significant changes in hierarchical organisation were observed in the subcortical network, with contributions from the visual and somatomotor networks. For Factor 2 (positive symptoms), the most prominent differences were found in the limbic and subcortical networks. Lastly, for Factor 3 (formal thought disorder and apathy), the most notable changes were observed in the limbic network (Supplementary Table 6). These findings suggest that different symptom dimensions in schizophrenia are associated with distinct patterns of hierarchical organisation in specific brain networks.

Hierarchical reconfiguration can classify between individuals with schizophrenia and controls

We determined whether differences in brain dynamics between schizophrenia and controls can be more effectively explained due to changes in brain hierarchy (as reflected in FDT deviations) or by other functional metrics in the literature (Functional Connectivity (FC) and Effective Connectivity (EC)). We trained an SVM classifier using the FC, the EC, the FDT deviations and a combination of EC and FDT (EC + FDT) as input. Our results indicate that the FDT input, together with the combination of EC + FDT inputs, achieve the highest accuracy among the classifiers (82.5 and 81.5%, respectively), surpassing the 73% obtained using EC and the 60% obtained using FC (Fig. 5). Furthermore, we repeated the same analysis ensuring the same number of input features for each model. For that, we performed a Principal Component Analysis and used the first ten principal components for the SVM classifiers (Supplementary Fig. 2). These results follow the same trend of performance as the full-dimensional inputs, with the highest accuracy obtained in the FDT and EC + FDT inputs (76 and 73.5%, respectively), followed by the EC (65%) and the FC (60.5%). Additionally, to assess whether incorporating temporal dynamics could further improve classification, we repeated the SVM analysis using features extracted through a sliding-window approach. For each window, we computed FC and estimated the corresponding whole-brain model to derive EC and FDT deviations, resulting in dynamic representations of all metrics. A PCA was again applied to reduce dimensionality, and the first ten components were used in the SVM. The results (Supplementary Fig. 3)

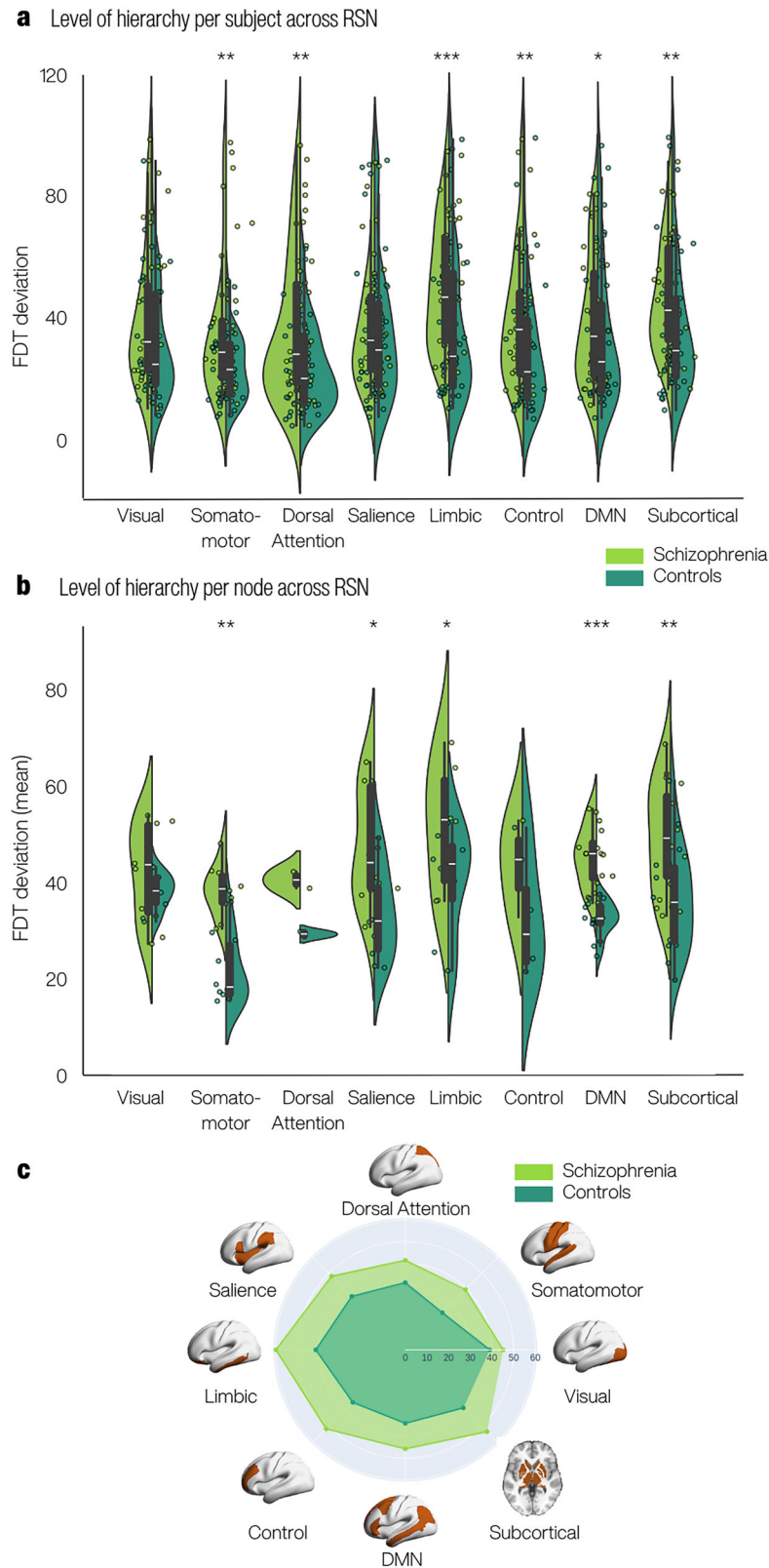


Fig. 3 Increased hierarchical organisation in some schizophrenia RSNs. Comparison of FDT deviation values between schizophrenia and control groups to identify the networks contributing to the difference in hierarchical organisation. **a** Boxplots illustrate the distribution of the average FDT values per subject for each RSN. **b** Boxplots illustrate the distribution of the average FDT values per node for each RSN. **c** Radar plot shows the mean FDT values per RSN for each group on the same scale, complemented with a brain render highlighting in orange the area of the corresponding network. All the reported p-values were corrected for multiple comparisons. * represents $p < 0.05$, ** represents $p < 0.01$ and *** represents $p < 0.001$.

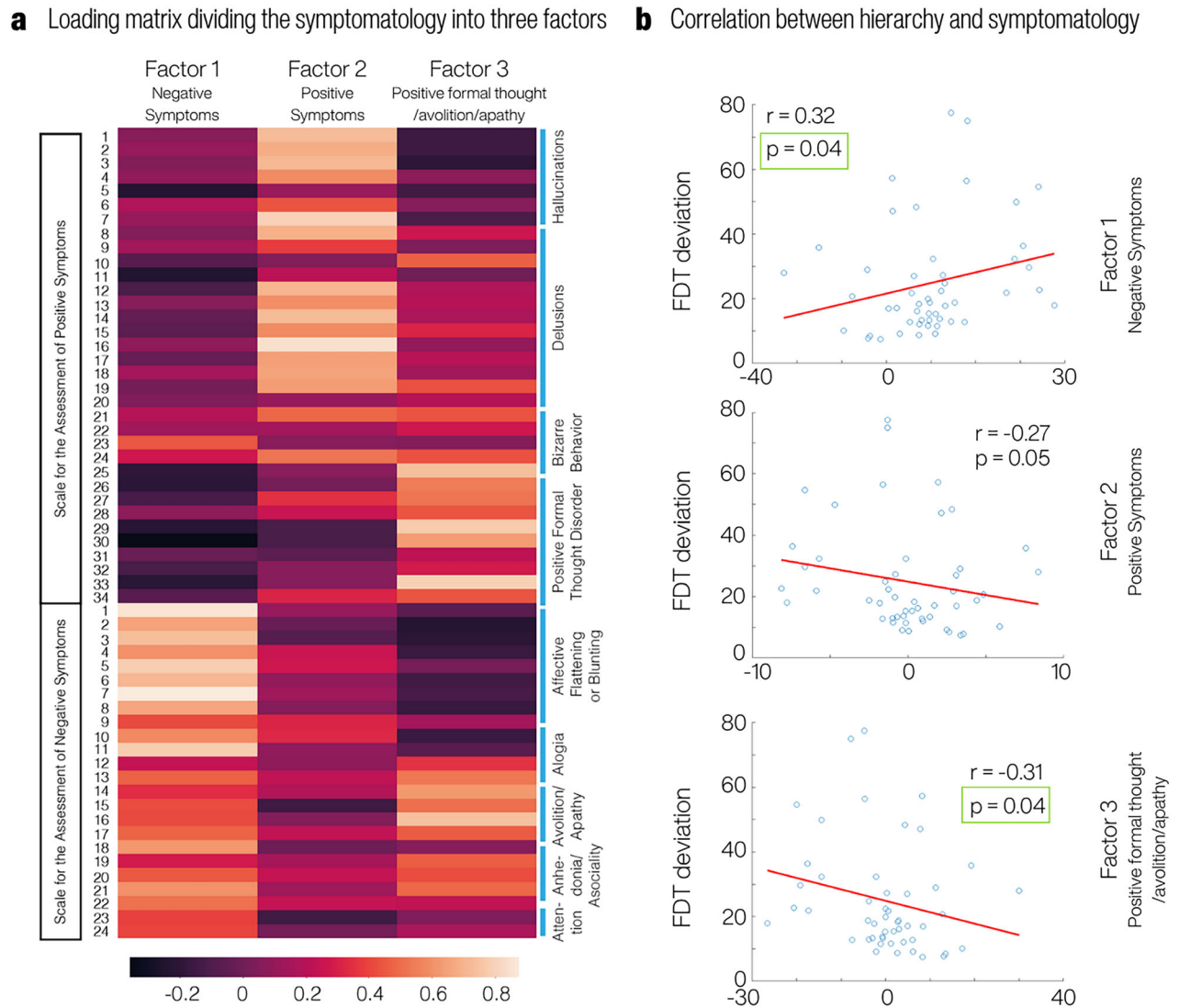


Fig. 4 The variability of the hierarchical organisation in schizophrenia correlates with symptom severity. Exploration of the correlation between the standard deviation of FDT deviation across brain regions in each subject and their symptomatology items evaluated using the SAPS and SANS scales. **a** Loading matrix of the three-factor solution derived from the exploratory factor analysis, including SAPS and SANS variables. Each row indicates an item on the scales. Interestingly, Factor 1 shows strong values for the SANS variables, Factor 2 for the SAPS, and Factor 3 for positive formal thought disorder and avolition/apathy items. **b** Correlation between the factor scores of each subject and standard deviation of their FDT deviation values.

showed consistent trends with the static analysis, with dynamic FDT and EC + FDT inputs achieving the highest classification accuracies (88 and 88.5%, respectively), supporting the relevance of hierarchical dynamics in distinguishing schizophrenia from controls.

Finally, focusing on the EC + FDT and FDT SVM models, we conducted an in-depth analysis by identifying the top 5 most influential features for the classification, corresponding to the highest coefficients of the model (Table 1). These nodes are primarily located within the subcortical and limbic networks, being these the regions previously reported to show most of the significant differences between the two groups (Fig. 3c, Supplementary Table 3). Moreover, the DMN and visual networks also appear to be highly important for the classification.

DISCUSSION

We integrated a whole-brain computational model with the fluctuation-dissipation theorem (FDT) to investigate whether the brain's hierarchical organisation differs in patients with

schizophrenia, using FDT deviations as a metric of hierarchy. Our analysis revealed consistently heightened organisation in schizophrenia, with significant differences observed in the somatomotor, dorsal attention, salience, limbic, control, DMN and subcortical networks. Moreover, these changes correlated with the severity of formal thought disorder, negative and positive symptoms. Finally, an SVM model demonstrated that including FDT in the input features allows for superior classification of schizophrenia patients versus controls.

At the whole-brain level, we found increased FDT deviation in schizophrenia. A deviation from the FDT is characteristic of a system departing from the equilibrium [45, 46], which is defined by asymmetrical interactions between its components and a hierarchically organised structure [29, 65]. Increased FDT deviation suggests an elevated level of non-equilibrium and more hierarchically organised brain dynamics in schizophrenia compared to controls, suggesting a stronger contribution of top-down processing [29]. Furthermore, our findings indicate increased variability of FDT deviation across nodes in schizophrenia, aligning

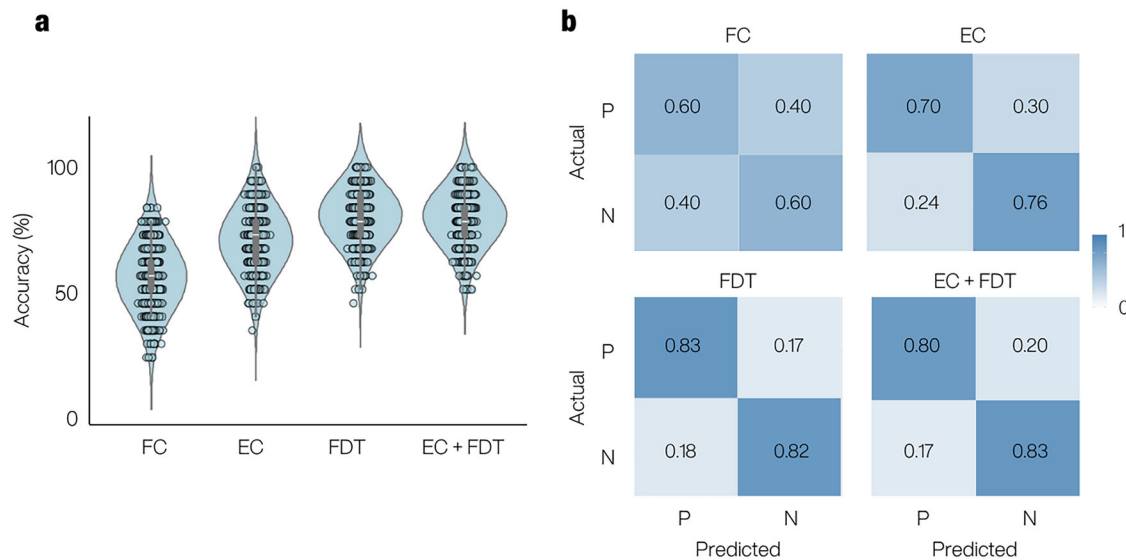


Fig. 5 Including hierarchical organisation features in a Support Vector Machine classification yields better accuracy than traditional functional or effective connectivity features. Comparison of the accuracy obtained using a SVM algorithm with different inputs (FC, EC, FDT and EC + FDT) to identify the most informative metrics. **a** Violin plots display the distribution of SVM accuracy across 1000 k-folds using FC, EC, FDT and EC + FDT data as inputs. **b** Confusion matrices illustrate the overall accuracy achieved corresponding to the distributions in (a), presented as percentages represented on a color scale. P stands for positive, N for negative.

Table 1. Subcortical, visual, limbic, and default mode regions are the most influential for accurate classification.

Node name	Corresponding RSN	Node name	Corresponding RSN
right inferior temporal	Limbic	right pericalcarine	Visual
right globus pallidus internus	Subcortical	right inferior temporal	Limbic
left nucleus accumbens	Subcortical	left pars orbitalis	DMN
right pericalcarine	Visual	right pericalcarine	Visual
right amygdala	Subcortical	right globus pallidus internus	Subcortical

This table presents the top 5 most important features obtained through SVM classification of the best performing models, indicating the relevance of specific nodes and their corresponding RSN, sorted in descending order. The higher the feature in the table, the greater the significance of the node in classification.

with previous research indicating that higher neural heterogeneity is a general characteristic of mental illness [67]. This adds to the growing evidence that psychiatric disorders exhibit greater heterogeneity, reinforcing the need for transdiagnostic approaches in mental health research. Specifically, we found that the higher levels of the hierarchy are occupied by the limbic, subcortical, DMN and control networks. These areas exhibit greater influence over the other RSNs, driving the orchestration and organising the functional dynamics to a higher extent than controls.

Previous studies have also shown differences in the whole-brain hierarchical organisation of networks in schizophrenia [38, 39], while others have highlighted reduced hierarchical organisation [29, 68]. This apparent discrepancy with our findings, which indicate increased hierarchical organisation, may stem from differences in the data and methods used to compute hierarchy. Specifically, Dong et al. [68] estimated hierarchy based on FC, which captures undirected statistical dependencies between brain regions. In contrast, our analysis relies on EC, which incorporates the directionality of interactions, potentially providing a different perspective on hierarchical organisation. Regarding the other study reporting reduced hierarchy [33], the authors approached the analysis from a non-stationarity perspective. They segmented each subject's data into multiple short time windows, thus combining hierarchical metrics with dynamic changes over time. Although they found significant group differences, these were

relatively small, likely due to the windowing approach, compared to our analysis, where we leverage the entire time series for each subject.

Notably, a previous study found that the connectivity between the DMN with other regions was more consistently present in individuals with schizophrenia than controls [69]. Moreover, Yang et al. [37] demonstrated that higher functional hierarchy in the DMN underlies the persistently observed elevated FC in studies of schizophrenia [17, 70, 71]. Increased connectivity between DMN and both the somatomotor and visual networks was also reported in [72]. This goes in line with our outcomes, emphasizing the important role of this network in schizophrenia. Regarding the subcortical network, Yang et al. [73] identified functional subcortical hierarchy disorganisation in drug-naïve schizophrenia patients, which normalized after antipsychotic treatment. Additionally, Sabarodien et al. [74] reported dysconnectivity within the subcortex in first-episode psychosis patients, which later extended to dysconnectivity between the cortex and subcortical systems in established schizophrenia. These findings are consistent with our results, emphasizing the involvement of the subcortical network in the disease. For the limbic and control networks, Xiang et al. [75] investigated functional gradients in schizophrenia, which have been proposed as a measure of hierarchical organisation. Interestingly, they found increased gradient scores in the limbic, control, and DMN networks, alongside decreases in the visual and somatomotor networks, findings that closely align with our results.

Our findings highlight correlations between the variability in hierarchical organisation in individuals with schizophrenia and the severity of negative symptoms, positive formal thought disorder and apathy. Previous studies have reported correlations between changes in DMN connectivity and negative symptoms [76, 77]. Hierarchical changes within this network could be affecting processes such as self-referential thinking and introspective cognition. Additionally, research has indicated that the somatomotor network can also impact negative symptoms [78]. Alterations in its hierarchical organisation could impact motor planning and execution, contributing to symptoms such as psychomotor retardation and speech abnormalities. Furthermore, dysregulation of the salience network has been associated with negative symptoms and motivational deficits in schizophrenia [16, 79], potentially leading to apathy and reduced responsiveness to environmental cues. These findings are consistent with our outcomes, suggesting that alterations in the hierarchical organisation of specific networks may underlie the manifestation of symptoms commonly observed in the disease. Notably, we also assessed whether the average FDT deviation across regions was associated with symptom severity but found no significant correlations (all p -values > 0.05). This lack of association may reflect the fact that averaging can obscure region-specific effects, as deviations in opposite directions across different brain areas may cancel each other out. In contrast, the variability in FDT captures the degree of imbalance across regions, which appears to be more relevant for symptom expression.

Finally, we employed a machine learning classification model to evaluate whether the differences in brain dynamics between schizophrenia and controls are better captured by alterations in brain hierarchy or by other functional metrics, such as FC and EC. The model demonstrated the highest performance when trained with FDT deviation features, being FDT alone or in combination with EC. This result suggests that disruptions in the hierarchical organisation of brain dynamics, as measured by FDT deviations, play a critical role in distinguishing individuals with schizophrenia from controls and provide more informative features than FC or EC alone. Beyond the previously reported networks to show the greatest differences between the two groups, the model also underscored the relevance of the visual and DMN networks, which were not prominently identified in the previous statistical analysis. This underscores the complementary nature of machine learning approaches in identifying patterns that may elude traditional statistical methods.

Our results are potentially compatible with shifts in the balance between excitation (E) and inhibition (I) mediated by NMDA receptor hypofunction implicated in schizophrenia [80–82]. Interestingly, previous research in primates using computational models proposed that variations in local recurrent excitation strength at different hierarchical levels account for the observed differences in neural activity time-scales across cortical regions [83–85]. To bridge between functional neuroimaging and neuronal-level alterations, a previous study constructed a biophysical model integrating the hierarchical brain organisation and E/I perturbations, which was able to predict the brain dynamics observed in the disease [37]. Moreover, Brau et al. [86] observed the effects of an NMDA antagonist in healthy controls, which led to increased network flexibility (i.e., higher reconfiguration of brain networks). Also using an NMDA antagonist for anaesthesia, Deco et al. [33] predicted heightened hierarchy in primates compared to their awake state. As a future step, it would be valuable to extend our framework by including receptor maps, such as in [87, 88], to obtain a deeper and more precise understanding of our findings.

Another possible link of our findings of disrupted hierarchical organisation in schizophrenia is with theories of impaired predictive coding. Predictive coding is inherently hierarchical, involving the interplay between top-down expectations and bottom-up sensory inputs to minimize prediction errors [89].

Deficits in this process, such as altered precision weighting of sensory information and predictions, have been implicated in schizophrenia symptomatology, including delusional thoughts [90], hallucinations [91] and altered sense of agency [92]. Although we do not directly measure predictive coding mechanisms, the patterns of functional hierarchy disruption and their correlation with clinical symptoms suggest that these mechanisms might be interconnected. This is because hierarchical organisation reflects how information is integrated and propagated across brain regions, and disruptions here could lead to improper balancing of sensory evidence and prior expectations, a core aspect of predictive coding dysfunction in schizophrenia.

The current study has several limitations. First, although consistent with comparable studies in the field [93, 94], the dataset analysed in this study is relatively small. Second, a potential limitation arises from the conceivable influence of medication on brain dynamics, which could impact the observed brain activity and subsequent results [95]. Third, in the parcellation employed in the analysis (i.e., the DK80 atlas [52]), the dorsal attention network is constituted by only two nodes and, thus, we refrain from making detailed interpretations when comparing groups by nodes. Finally, another limitation is that the SC matrix was derived from a separate normative sample of healthy participants, rather than from the same individuals in the main analysis. This approach, consistent with prior work [96, 97], was necessary due to the unavailability of subject-specific diffusion data. Importantly, EC was individually optimized for each participant, allowing the model to capture subject-specific dynamics and reduce potential biases from using normative SC.

In summary, we used a computational whole-brain model and the violations of the FDT and found elevated hierarchical brain organisation in schizophrenia compared to controls both across the whole-brain and RSNs. Furthermore, we found that the changes in hierarchy are correlated with negative symptoms, positive formal thought disorder and apathy. Finally, through SVM classification, we demonstrated that including FDT deviations in the input resulted in superior classification accuracy than individual metrics (i.e., FC, EC). Overall, this framework can be potentially used as a model-based biomarker to differentiate schizophrenia from healthy controls. Importantly, this inquiry is not limited to schizophrenia alone but opens up broader perspectives for understanding the hierarchical brain organisation of other psychiatric conditions and different brain states.

DATA AVAILABILITY

Raw data are available at openneuro.org/datasets/ds000030/. Preprocessed data and scripts are available upon request.

CODE AVAILABILITY

Code used to analyse the data is available from https://github.com/lrenacero/FDT_schizophrenia.git.

REFERENCES

1. Kay SR, Fiszbein A, Opler LA. The positive and negative syndrome scale (PANSS) for schizophrenia. *Schizophr Bull.* 1987;13:261–76.
2. Mueser KT, McGurk SR. Schizophrenia. *Lancet.* 2004;363:2063–72.
3. Glahn DC, Laird AR, Ellison-Wright I, Thelen SM, Robinson JL, Lancaster JL, et al. Meta-analysis of gray matter anomalies in schizophrenia: application of anatomical likelihood estimation and network analysis. *Biol Psychiatry.* 2008;64:774–81.
4. Kubicki M, McCarley RW, Shenton ME. Evidence for white matter abnormalities in schizophrenia. *Curr Opin Psychiatry.* 2005;18:121–34.
5. Chan RC, Di X, McAlonan GM, Gong QY. Brain anatomical abnormalities in high-risk individuals, first-episode, and chronic schizophrenia: an activation likelihood estimation meta-analysis of illness progression. *Schizophr Bull.* 2011;37:177–88.
6. Davidson LL, Heinrichs RW. Quantification of frontal and temporal lobe brain-imaging findings in schizophrenia: a meta-analysis. *Psychiatry Res.* 2003;122:69–87.

7. Honea R, Crow TJ, Passingham D, Mackay CE. Regional deficits in brain volume in schizophrenia: a meta-analysis of voxel-based morphometry studies. *Am J Psychiatry*. 2005;162:2233–45.
8. Bora E, Fornito A, Radua J, Walterfang M, Seal M, Wood SJ, et al. Neuroanatomical abnormalities in schizophrenia: a multimodal voxelwise meta-analysis and meta-regression analysis. *Schizophr Res*. 2011;127:46–57.
9. Ellison-Wright I, Bullmore E. Anatomy of bipolar disorder and schizophrenia: a meta-analysis. *Schizophr Res*. 2010;117:1–12.
10. Adriano F, Spoletini I, Caltagirone C, Spalletta G. Updated meta-analyses reveal thalamus volume reduction in patients with first-episode and chronic schizophrenia. *Schizophr Res*. 2010;123:1–14.
11. Wylie KP, Tregellas JR. The role of the insula in schizophrenia. *Schizophr Res*. 2010;123:93–104.
12. Di X, Chan RC, Gong QY. White matter reduction in patients with schizophrenia as revealed by voxel-based morphometry: an activation likelihood estimation meta-analysis. *Prog Neuropsychopharmacol Biol Psychiatry*. 2009;33:1390–4.
13. Smitha KA, Akhil Raja K, Arun KM, Rajesh PG, Thomas B, Kapilamoorthy TR, et al. Resting state fMRI: a review on methods in resting state connectivity analysis and resting state networks. *Neuroradiol J*. 2017;30:305–17.
14. Filippi M, Spinelli EG, Cividini C, Agosta F. Resting state dynamic functional connectivity in neurodegenerative conditions: a review of magnetic resonance imaging findings. *Front Neurosci*. 2019;13:657.
15. Bressler SL, Menon V. Large-scale brain networks in cognition: emerging methods and principles. *Trends Cogn Sci*. 2010;14:277–90.
16. Palaniyappan L, Liddle PF. Does the salience network play a cardinal role in psychosis? An emerging hypothesis of insular dysfunction. *J Psychiatry Neurosci*. 2012;37:17–27.
17. Zhou Y, Liang M, Tian L, Wang K, Hao Y, Liu H, et al. Functional disintegration in paranoid schizophrenia using resting-state fMRI. *Schizophr Res*. 2007;97:194–205.
18. Whitfield-Gabrieli S, Thermenos HW, Milanovic S, Tsuang MT, Faraone SV, McCarley RW, et al. Hyperactivity and hyperconnectivity of the default network in schizophrenia and in first-degree relatives of persons with schizophrenia. *Proc Natl Acad Sci USA*. 2009;106:1279–84.
19. Camchong J, MacDonald AW 3rd, Bell C, Mueller BA, Lim KO. Altered functional and anatomical connectivity in schizophrenia. *Schizophr Bull*. 2011;37:640–50.
20. Dong D, Wang Y, Chang X, Luo C, Yao D. Dysfunction of large-scale brain networks in schizophrenia: a meta-analysis of resting-state functional connectivity. *Schizophr Bull*. 2018;44:168–81.
21. Penadés R, Segura B, Inguanzo A, García-Rizo C, Catalán R, Masana G, et al. Cognitive remediation and brain connectivity: a resting-state fMRI study in patients with schizophrenia. *Psychiatry Res Neuroimaging*. 2020;303:111140.
22. Jia Y, Gu H-G. Identifying nonlinear dynamics of brain functional networks of patients with schizophrenia by sample entropy. *Nonlinear Dynamics*. 2019;96:2327–40.
23. Tandon R, Nasrallah H, Akbarian S, Carpenter WT Jr, DeLisi LE, Gaebel W, et al. The schizophrenia syndrome, circa 2024: what we know and how that informs its nature. *Schizophr Res*. 2024;264:1–28.
24. Braff DL. Information processing and attention dysfunctions in schizophrenia. *Schizophr Bull*. 1993;19:233–59.
25. Rubinov M, Bullmore E. Schizophrenia and abnormal brain network hubs. *Dialogues Clin Neurosci*. 2013;15:339–49.
26. Chen Y. Abnormal visual motion processing in schizophrenia: a review of research progress. *Schizophr Bull*. 2011;37:709–15.
27. Iglesias-Parro S, Ruiz de Miras J, Soriano MF, Ibáñez-Molina AJ. Integration-segregation dynamics in functional networks of individuals diagnosed with schizophrenia. *Eur J Neurosci*. 2023;57:1748–62.
28. Kringelbach ML, Sanz Perl Y, Deco G. The thermodynamics of mind. *Trends Cogn Sci*. 2024;28:568–81.
29. Deco G, Sanz Perl Y, de la Fuente L, Sitt JD, Yeo BTT, Tagliazucchi E, et al. The arrow of time of brain signals in cognition: potential intriguing role of parts of the default mode network. *Netw Neurosci*. 2023;7:966–98.
30. Huntenburg JM, Bazin PL, Margulies DS. Large-scale gradients in human cortical organization. *Trends Cogn Sci*. 2018;22:21–31.
31. Taylor P, Hobbs JN, Burroni J, Siegelmann HT. The global landscape of cognition: hierarchical aggregation as an organizational principle of human cortical networks and functions. *Sci Rep*. 2015;5:18112.
32. Sanz Perl Y, Bocaccio H, Pallavicini C, Pérez-Ipiña I, Laureys S, Laufs H, et al. Nonequilibrium brain dynamics as a signature of consciousness. *Phys Rev E*. 2021;104:014411.
33. Deco G, Sanz Perl Y, Bocaccio H, Tagliazucchi E, Kringelbach ML. The INSIDEOUT framework provides precise signatures of the balance of intrinsic and extrinsic dynamics in brain states. *Commun Biol*. 2022;5:572.
34. Kringelbach ML, Perl YS, Tagliazucchi E, Deco G. Toward naturalistic neuroscience: mechanisms underlying the flattening of brain hierarchy in movie-watching compared to rest and task. *Sci Adv*. 2023;9:eade6049.
35. Lynn CW, Cornblath EJ, Papadopoulos L, Bertolero MA, Bassett DS. Broken detailed balance and entropy production in the human brain. *Proc Natl Acad Sci USA*. 2021;118:e2109889118.
36. Lynall ME, Bassett DS, Kerwin R, McKenna PJ, Kitzbichler M, Muller U, et al. Functional connectivity and brain networks in schizophrenia. *J Neurosci*. 2010;30:9477–87.
37. Yang GJ, Murray JD, Wang XJ, Glahn DC, Pearlson GD, Repovs G, et al. Functional hierarchy underlies preferential connectivity disturbances in schizophrenia. *Proc Natl Acad Sci USA*. 2016;113:E219–28.
38. Wengler K, Goldberg AT, Chahine G, Horga G. Distinct hierarchical alterations of intrinsic neural timescales account for different manifestations of psychosis. *Elife*. 2020;9:e56151.
39. Mastrandrea R, Piras F, Gabrielli A, Banaj N, Caldarelli G, Spalletta G, et al. The unbalanced reorganization of weaker functional connections induces the altered brain network topology in schizophrenia. *Sci Rep*. 2021;11:15400.
40. Dickie EW, Shahab S, Hawco C, Miranda D, Herman G, Argyelan M, et al. Robust hierarchically organized whole-brain patterns of dysconnectivity in schizophrenia spectrum disorders observed after personalized intrinsic network topography. *Hum Brain Mapp*. 2023;44:5153–66.
41. Barbalat G, Chambon V, Domenech PJ, Ody C, Koechlin E, Franck N, et al. Impaired hierarchical control within the lateral prefrontal cortex in schizophrenia. *Biol Psychiatry*. 2011;70:73–80.
42. Holmes A, Levi PT, Chen YC, Chopra S, Aquino KM, Pang JC, et al. Disruptions of hierarchical cortical organization in early psychosis and schizophrenia. *Biol Psychiatry Cogn Neurosci Neuroimaging*. 2023;8:1240–50.
43. Dong D, Yao D, Wang Y, Hong SJ, Genon S, Xin F, et al. Compressed sensorimotor-transmodal hierarchical organization in schizophrenia. *Psychol Med*. 2023;53:771–84.
44. Deco G, Lynn CW, Sanz Perl Y, Kringelbach ML. Violations of the fluctuation-dissipation theorem reveal distinct nonequilibrium dynamics of brain states. *Phys Rev E*. 2023;108:064410.
45. Onsager L. Reciprocal relations in irreversible processes. I. *Physical Review*. 1931;37:405–26.
46. Kubo R. The Fluctuation-dissipation theorem. *Reports on Progress in Physics*. 2002;29:255.
47. Bilder R, Poldrack R, Cannon T, London E, Freimer N, Congdon E, et al. UCLA consortium for neuropsychiatric phenomics LA5c study. *OpenNeuro*; 2018.
48. Poldrack RA, Congdon E, Triplett W, Gorgolewski KJ, Karlsgodt KH, Mumford JA, et al. A phenome-wide examination of neural and cognitive function. *Sci Data*. 2016;3:160110.
49. Esteban O, Markiewicz CJ, Blair RW, Moodie CA, Isik AI, Erramuzpe A, et al. fMRIPrep: a robust preprocessing pipeline for functional MRI. *Nat Methods*. 2019;16:111–6.
50. Gorgolewski K, Burns CD, Madison C, Clark D, Halchenko YO, Waskom ML, et al. Nipype: a flexible, lightweight and extensible neuroimaging data processing framework in python. *Front Neuroinform*. 2011;5:13.
51. Pruim RHR, Mennes M, van Rooij D, Llera A, Buitelaar JK, Beckmann CF. ICA-AROMA: a robust ICA-based strategy for removing motion artifacts from fMRI data. *Neuroimage*. 2015;112:267–77.
52. Deco G, Vidaurre D, Kringelbach ML. Revisiting the global workspace orchestrating the hierarchical organization of the human brain. *Nat Hum Behav*. 2021;5:497–511.
53. Thomas C, Ye FQ, Irfanoglu MO, Modi P, Saleem KS, Leopold DA, et al. Anatomical accuracy of brain connections derived from diffusion MRI tractography is inherently limited. *Proc Natl Acad Sci USA*. 2014;111:16574–9.
54. Horn A, Neumann WJ, Degen K, Schneider GH, Kühn AA. Toward an electrophysiological “sweet spot” for deep brain stimulation in the subthalamic nucleus. *Hum Brain Mapp*. 2017;38:3377–90.
55. Horn A, Blankenburg F. Toward a standardized structural-functional group connectome in MNI space. *Neuroimage*. 2016;124:310–22.
56. Schilling KG, Daducci A, Maier-Hein K, Poupon C, Houde JC, Nath V, et al. Challenges in diffusion MRI tractography - lessons learned from international benchmark competitions. *Magn Reson Imaging*. 2019;57:194–209.
57. Maier-Hein KH, Neher PF, Houde JC, Côté MA, Garyfallidis E, Zhong J, et al. Author correction: the challenge of mapping the human connectome based on diffusion tractography. *Nat Commun*. 2019;10:5059.
58. Crisanti A, Ritort F. Violation of the fluctuation-dissipation theorem in glassy systems: basic notions and the numerical evidence. *J Phys A: Math Gen*. 2003;36:R181–R290.
59. Deco G, Kringelbach ML, Jirsa VK, Ritter P. The dynamics of resting fluctuations in the brain: metastability and its dynamical cortical core. *Sci Rep*. 2017;7:3095.
60. Deco G, Ponce-Alvarez A, Hagmann P, Romani GL, Mantini D, Corbetta M. How local excitation-inhibition ratio impacts the whole brain dynamics. *J Neurosci*. 2014;34:7886–98.

61. Lord LD, Expert P, Atasoy S, Roseman L, Rapuano K, Lambiotte R, et al. Dynamical exploration of the repertoire of brain networks at rest is modulated by psilocybin. *Neuroimage*. 2019;199:127–42.
62. Yeo BT, Krienen FM, Sepulcre J, Sabuncu MR, Lashkari D, Hollinshead M, et al. The organization of the human cerebral cortex estimated by intrinsic functional connectivity. *J Neurophysiol*. 2011;106:1125–65.
63. Schöttner M, Bolton TAW, Patel J, Nahálka AT, Vieira S, Hagmann P. Exploring the latent structure of behavior using the Human Connectome Project's data. *Sci Rep*. 2023;13:713.
64. Hochberg Y, Benjamini Y. More powerful procedures for multiple significance testing. *Stat Med*. 1990;9:811–8.
65. de la Fuente LA, Zamberlan F, Bocaccio H, Kringelbach M, Deco G, Perl YS, et al. Temporal irreversibility of neural dynamics as a signature of consciousness. *Cereb Cortex*. 2023;33:1856–65.
66. Aguilera M, Igarashi M, Shimazaki H. Nonequilibrium thermodynamics of the asymmetric Sherrington-Kirkpatrick model. *Nat Commun*. 2023;14:3685.
67. Segal A, Parkes L, Aquino K, Kia SM, Wolfers T, Franke B, et al. Regional, circuit and network heterogeneity of brain abnormalities in psychiatric disorders. *Nat Neurosci*. 2023;26:1613–29.
68. Dong D, Luo C, Guell X, Wang Y, He H, Duan M, et al. Compression of cerebellar functional gradients in schizophrenia. *Schizophr Bull*. 2020;46:1282–95.
69. Jafri MJ, Pearlson GD, Stevens M, Calhoun VD. A method for functional network connectivity among spatially independent resting-state components in schizophrenia. *Neuroimage*. 2008;39:1666–81.
70. Liu H, Kaneko Y, Ouyang X, Li L, Hao Y, Chen EY, et al. Schizophrenic patients and their unaffected siblings share increased resting-state connectivity in the task-negative network but not its anticorrelated task-positive network. *Schizophr Bull*. 2012;38:285–94.
71. Hu ML, Zong XF, Mann JJ, Zheng JJ, Liao YH, Li ZC, et al. A review of the functional and anatomical default mode network in schizophrenia. *Neurosci Bull*. 2017;33:73–84.
72. Orliac F, Delamillieure P, Delcroix N, Naveau M, Brazo P, Razafimandimby A, et al. Network modeling of resting state connectivity points towards the bottom up theories of schizophrenia. *Psychiatry Res Neuroimaging*. 2017;266:19–26.
73. Yang C, Zhang W, Liu J, Yao L, Bishop JR, Lencer R, et al. Disrupted subcortical functional connectome gradient in drug-naïve first-episode schizophrenia and the normalization effects after antipsychotic treatment. *Neuropsychopharmacology*. 2023;48:789–96.
74. Sabarodin K, Razi A, Chopra S, Tran N, Pozaruk A, Chen Z, et al. Frontostriatthalamic effective connectivity and dopaminergic function in the psychosis continuum. *Brain*. 2023;146:372–86.
75. Xiang J, Ma C, Chen X, Cheng C. Investigating connectivity gradients in schizophrenia: integrating functional, structural, and genetic perspectives. *Brain Sci*. 2025;15:179.
76. Hare SM, Ford JM, Mathalon DH, Damaraju E, Bustillo J, Belger A, et al. Salience-default mode functional network connectivity linked to positive and negative symptoms of schizophrenia. *Schizophr Bull*. 2019;45:892–901.
77. Wang X, Chang Z, Wang R. Opposite effects of positive and negative symptoms on resting-state brain networks in schizophrenia. *Commun Biol*. 2023;6:279.
78. Bernard JA, Goen JRM, Maldonado T. A case for motor network contributions to schizophrenia symptoms: evidence from resting-state connectivity. *Hum Brain Mapp*. 2017;38:4535–45.
79. Menon V. Large-scale brain networks and psychopathology: a unifying triple network model. *Trends Cogn Sci*. 2011;15:483–506.
80. Uhlhaas PJ, Singer W. Abnormal neural oscillations and synchrony in schizophrenia. *Nat Rev Neurosci*. 2010;11:100–13.
81. Jardri R, Denève S. Circular inferences in schizophrenia. *Brain*. 2013;136:3227–41.
82. Schobel SA, Chaudhury NH, Khan UA, Paniagua B, Styner MA, Asllani I, et al. Imaging patients with psychosis and a mouse model establishes a spreading pattern of hippocampal dysfunction and implicates glutamate as a driver. *Neuron*. 2013;78:81–93.
83. Wang XJ. Synaptic reverberation underlying mnemonic persistent activity. *Trends Neurosci*. 2001;24:455–63.
84. Homayoun H, Moghaddam B. NMDA receptor hypofunction produces opposite effects on prefrontal cortex interneurons and pyramidal neurons. *J Neurosci*. 2007;27:11496–500.
85. Murray JD, Bernacchia A, Freedman DJ, Romo R, Wallis JD, Cai X, et al. A hierarchy of intrinsic timescales across primate cortex. *Nat Neurosci*. 2014;17:1661–3.
86. Braun U, Schäfer A, Bassett DS, Rausch F, Schweiger JI, Bilek E, et al. Dynamic brain network reconfiguration as a potential schizophrenia genetic risk mechanism modulated by NMDA receptor function. *Proc Natl Acad Sci USA*. 2016;113:12568–73.
87. Deco G, Cruzat J, Cabral J, Knudsen GM, Carhart-Harris RL, Whybrow PC, et al. Whole-brain multimodal neuroimaging model using serotonin receptor maps explains non-linear functional effects of LSD. *Curr Biol*. 2018;28:3065–74.e6.
88. Vohryzek J, Cabral J, Lord LD, Fernandes HM, Roseman L, Nutt DJ, et al. Brain dynamics predictive of response to psilocybin for treatment-resistant depression. *Brain Commun*. 2024;6:fcae049.
89. Friston K. A theory of cortical responses. *Philos Trans R Soc Lond B Biol Sci*. 2005;360:815–36.
90. Corlett PR, Murray GK, Honey GD, Aitken MR, Shanks DR, Robbins TW, et al. Disrupted prediction-error signal in psychosis: evidence for an associative account of delusions. *Brain*. 2007;130:2387–400.
91. Blakemore SJ, Smith J, Steel R, Johnstone CE, Frith CD. The perception of self-produced sensory stimuli in patients with auditory hallucinations and passivity experiences: evidence for a breakdown in self-monitoring. *Psychol Med*. 2000;30:1131–9.
92. Voss M, Moore J, Hauser M, Gallinat J, Heinz A, Haggard P. Altered awareness of action in schizophrenia: a specific deficit in predicting action consequences. *Brain*. 2010;133:3104–12.
93. Mana L, Vila-Vidal M, Köckeritz C, Aquino K, Fornito A, Kringelbach ML, et al. Using in silico perturbational approach to identify critical areas in schizophrenia. *Cereb Cortex*. 2023;33:7642–58.
94. Guan S, Wan D, Zhao R, Canario E, Meng C, Biswal BB. The complexity of spontaneous brain activity changes in schizophrenia, bipolar disorder, and ADHD was examined using different variations of entropy. *Hum Brain Mapp*. 2023;44:94–118.
95. Takahashi T, Cho RY, Mizuno T, Kikuchi M, Murata T, Takahashi K, et al. Anti-psychotics reverse abnormal EEG complexity in drug-naïve schizophrenia: a multiscale entropy analysis. *Neuroimage*. 2010;51:173–82.
96. Deco G, Kringelbach ML. Turbulent-like dynamics in the human brain. *Cell Rep*. 2020;33:108471.
97. Dagnino PC, Escrichs A, López-González A, Gosseries O, Annen J, Sanz Perl Y, et al. Re-awakening the brain: forcing transitions in disorders of consciousness by external in silico perturbation. *PLoS Comput Biol*. 2024;20:e1011350.

ACKNOWLEDGEMENTS

I.A.P. and A.E. are supported by grant PID2022-136216NB-I00 funded by MICIU/AEI/10.13039/501100011033 and by 'ERDF A way of making Europe', 'ERDF', 'EU'. P.D. is supported by the AGAUR FI-SDUR Grant (no. 2022 FISDU 00229). Y.S.P. is supported by the project NEurological MEchanismS of Injury, and Sleep-like cellular dynamics (NEMESIS; ref. 101071900) funded by the EU ERC Synergy Horizon Europe. M.L.K. is supported by the Centre for Eudaimonia and Human Flourishing (funded by the Pettit and Carlsberg Foundations) and the Center for Music in the Brain (funded by the Danish National Research Foundation, DNRF117). P.J.U. is supported by the project MR/L011689/1 from the Medical Research Council (MRC). G.D. is supported by grant no. PID2022-136216NB-I00 funded by MICIU/AEI/10.13039/501100011033 and by 'ERDF A way of making Europe', 'ERDF', 'EU, Project NEurological MEchanismS of Injury, and Sleep-like cellular dynamics (NEMESIS; ref. 101071900) funded by the EU ERC Synergy Horizon Europe, and AGAUR research support grant (ref. 2021 SGR 00917) funded by the Department of Research and Universities of the Generalitat of Catalunya.

AUTHOR CONTRIBUTIONS

IA-P: Conceptualization; Formal analysis; Investigation; Methodology; Project administration; Software; Validation; Visualization; Writing—original draft; Writing—review & editing. AE: Conceptualization; Formal analysis; Funding acquisition; Investigation; Resources; Supervision; Validation; Writing—review & editing. PCD: Formal analysis; Investigation; Resources; Software; Validation; Writing—review & editing. YSP: Conceptualization; Formal analysis; Investigation; Methodology; Resources; Software; Supervision; Validation; Writing—review & editing. MLK: Methodology; Resources; Software; Validation; Writing—review & editing. PJU: Resources; Writing—review & editing. GD: Conceptualization; Funding acquisition; Investigation; Methodology; Project administration; Resources; Software; Supervision; Validation; Writing—review & editing.

COMPETING INTERESTS

The authors declare no competing interest.

ETHICS APPROVAL AND CONSENT TO PARTICIPATE

All methods were performed in accordance with the relevant guidelines and regulations. The resting-state fMRI data analyzed in this study were obtained from the UCLA Consortium for Neuropsychiatric Phenomics LA5c Study (openneuro.org/datasets/ds000030), which was approved by the University of California Los Angeles Institutional Review Board. Written informed consent was obtained from all participants by the original investigators.

CONSENT FOR PUBLICATION

Not applicable, as the study used anonymized, publicly available data.

ADDITIONAL INFORMATION

Supplementary information The online version contains supplementary material available at <https://doi.org/10.1038/s41398-025-03584-0>.

Correspondence and requests for materials should be addressed to Irene Acero-Pousa.

Reprints and permission information is available at <http://www.nature.com/reprints>

Publisher's note Springer Nature remains neutral with regard to jurisdictional claims in published maps and institutional affiliations.



Open Access This article is licensed under a Creative Commons Attribution-NonCommercial-NoDerivatives 4.0 International License, which permits any non-commercial use, sharing, distribution and reproduction in any medium or format, as long as you give appropriate credit to the original author(s) and the source, provide a link to the Creative Commons licence, and indicate if you modified the licensed material. You do not have permission under this licence to share adapted material derived from this article or parts of it. The images or other third party material in this article are included in the article's Creative Commons licence, unless indicated otherwise in a credit line to the material. If material is not included in the article's Creative Commons licence and your intended use is not permitted by statutory regulation or exceeds the permitted use, you will need to obtain permission directly from the copyright holder. To view a copy of this licence, visit <http://creativecommons.org/licenses/by-nc-nd/4.0/>.

© The Author(s) 2025